DOI: 10.1002/ejic.200700320

Fe^{II} Bistable Materials with Dissymmetrical Ligands: Synthesis, Crystal Structure, Magnetic and Mössbauer Properties of Fe^{II} Complexes Based on N_4 Schiff Bases Possessing 2-Pyridyl and 1-R-Imidazol-2-yl Rings[‡]

Nicolas Bréfuel,*[a] and Sergiu Shova,[a][‡‡] and Jean-Pierre Tuchagues*[a]

Keywords: Schiff bases / N ligands / Iron / Spin crossover / Magnetic properties / Mössbauer spectroscopy

The synthesis and characterization of two symmetrical Fe^{II} complexes, $[FeL^{B4}(NCS)_2]$, **1**, and $[FeL^{B5}(NCS)_2]$, **2** {L^{Bx} = *N*,*N*′-bis[(2-*N*-R-imidazol-1-yl)methylene]-2,2-dimethylpropane-1,3-diamine ligands; **1**: *x* = 4, R = H; **2**: *x* = 5, R = Me} are reported. Whereas the tetradentate ligand L^{B4} is planar in **1**, the X-ray structure of **2** illustrates the folded conformation of L^{B5}. Ferrous $[FeL^{Ex}(NCS)_2]$ complexes were synthesized {L^{Ex} = *N*-[(1-*N*-R^2-imidazol-2-yl)methylene]-*N*′-(1-pyridin-2-yl-ethylidene)-2,2-R^1-propane-1,3-diamine; **3**: *x* = 1, R^1 = H, R^2 = H; **4**: *x* = 2, R^1 = H, R^2 = Me; **5**: *x* = 3, R^1 = Me, R^2 = H; **6**: *x* = 4, R^1 = Me, R^2 = Me}. These dissymmetrical Schiff bases, possessing pyridine and imidazole rings, are obtained through the reaction of 2-methyl-2-pyridin-2-yl-hexahydropyrimidine (R^1 = H; **3**, **4**) or 2,5,5-trimethyl-2-pyridin-2-yl-hexahydropyrimidine (R^1 = Me; **5**, **6**) aminals with imidazole-2-carboxaldehyde (R^2 = H: **3**, **5**) or 1-*N*-methylimidazole-2-carboxaldehyde (R^2 = Me: **4**, **6**) and iron(II) thiocyanate. Single-crystal X-ray structures were determined for $[FeL^{E1}(NCS)_2]$ **3** $[FeL^{E3}(NCS)_2]$ **5** and $[FeL^{E4}(NCS)_2]$ **6**; these complexes are in the low-spin state at 180 K. Magnetic susceptibility and Mössbauer measurements showed a smooth and incomplete spin crossover involving ca. 50 % of the iron centres between 200 and 400 K for **5** and **6**; **3** and **4** remain low spin up to 350 K; the slight $\chi_M T$ increase between 350 and 400 K results from the onset of spin crossover for **3** and **4**. The spin crossover properties in the $[FeL^{Ex}(NCS)_2]$ series may thus be tuned by the ligand substituents: by changing R^1 from H (for **3**, **4**) to Me (for **5**, **6**) the spin crossover is lowered from above 400 K to ca. 350 K; the effect of the imidazolyl substituent is weaker: by changing R^2 from H (for **5**) to Me (for **6**) the spin crossover temperature is lowered by ca. 35 K. The electronic effect of the highly conjugated Fe–N=C–C=N– imidazolyl fragment overpasses and qualitatively and quantitatively modifies the effects of R^1 and R^2.

Introduction

Most iron(II) complexes have octahedral geometry, and depending on the strength of the ligand field, either the low-spin (LS) or the high-spin (HS) electronic configuration is observed. For some Fe^{II} complexes, mainly those characterized by an $[FeN_6]$ core, the ligand field is intermediate and allows a LS (S = 0, $^1A_{1g}$) ↔ HS (S = 2, $^5T_{2g}$) spin crossover (SC) that may be induced by a variation in temperature, pressure or light irradiation.[1] Slight modifications to the ligand(s) may provide conditions that do or do not favour SC, depending on the balance between the ligand field and the mean spin-pairing energy. Whereas the phenomenon is mainly molecular in solution, intermolecular interactions, such as π–π staking or hydrogen bonds between complex molecules, are the key for observing cooperative transition in the solid state, as a result of the supramolecular structure.[2] Such a behaviour, evidenced by thermal hysteresis of the magnetic properties, is attractive owing to the potential technological applications of these materials in molecular electronics and memory devices.[3]

In previous studies, we showed that a rational approach for the design of SC materials allows tuning of the ligand field by combination, in a same tetradentate Schiff base ligand, of both the "strong ligand field" pyridine moiety and the "weak ligand field" imidazole ring.[4] Reaction between the isolated aminal-type ligands 2-methyl-2-pyridin-2-yl-hexahydropyrimidine (R^1 = H) or 2,5,5-trimethyl-2-pyridin-2-yl-hexahydropyrimidine (R^1 = Me) and 2-R^2-imidazole-4-carboxaldehyde, in the presence of iron(II) thiocyanate, led to the $[FeL^{Cx}(NCS)_2]$ complexes {L^{Cx} = *N*-[(2-R^2-1H-imidazol-4-yl)methylene]-*N*′-(1-pyridin-2-ylethylidene)-2,2-R^1-propane-1,3-diamine (R^1 = H, Me; R^2 = H, Me, Ph)}.[4a] Because the complexes in the $[FeL^{Cx}(NCS)_2]$ family exhibit only partial SC in the 60–400 K temperature range, we explored the $[FeL^{Dx}(NCX)_2]$ (X = S, Se) series

[‡] Fe^{II} Bistable Materials with Dissymmetrical Ligands, 3. Part 1, ref.[4a]; part 2, ref.[4b]

[a] Laboratoire de Chimie de Coordination du CNRS, UPR 8241
205 route de Narbonne, 31077 Toulouse Cedex, France
Fax: +33-561-553003
E-mail: brefuel@lcc-toulouse.fr
jean-pierre.tuchagues@lcc-toulouse.fr
[‡‡]On leave from the Institute of Applied Physics, Academy of Sciences of Moldova,
Academiei str. 3. 2028 Chisinau, Moldova

Supporting information for this article is available on the WWW under http://www.eurjic.org or from the author.

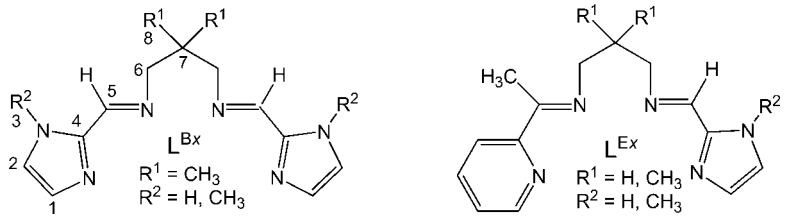

Figure 1. Schematic drawing of the L^{Bx} and L^{Ex} ligands (R^1 = H, Me; R^2 = H, Me).

where the terminal imidazolyl fragment of L^{Dx} originates from 5-methyl-4-formylimidazole.[4b] The complexes in the corresponding $[FeL^{Dx}(NCX)_2]$ series exhibit steeper SC, with hysteresis or with two steps, depending on the pseudohalide ligands (NCS or NCSe) and on the R^1 substituent of the propyl chain. Detailed structural studies revealed the prominent role of the hydrogen bond network in the occurrence of steep SC, as underlined by the hysteresis evidenced through their magnetic study.[4b]

In this paper, we report the synthesis and characterization of six ferrous materials including: (1) two HS complexes of general formula $[FeL^{Bx}(NCS)_2]$ {L^{Bx} = *N*,*N*′-bis-[(2-*N*-R-imidazol-1-yl)methylene]-2,2-dimethylpropane-1,3-diamine ligands (Figure 1); **1**: x = 4, R = H; **2**: x = 5, R = Me} and (2) a series of ferrous complexes $[FeL^{Ex}(NCS)_2]$ {L^{Ex} = *N*-[(1-*N*-R^2-imidazol-2-yl)methylene]-*N*′-(1-pyridin-2-ylethylidene)-2,2-R^1-propane-1,3-diamine ligands (Figure 1); **3**: x = 1, R^1 = H, R^2 = H; **4**: x = 2, R^1 = H, R^2 = Me; **5**: x = 3, R^1 = Me, R^2 = H; **6**: x = 4, R^1 = Me, R^2 = Me}. The molecular structure of these materials was investigated by single-crystal X-ray diffraction, and their electronic properties were explored by variable-temperature magnetic susceptibility and Mössbauer studies.

Results

Description of the Structures

The molecular structures along with the main geometric characteristics of complexes **2**, **3**, **5** and **6** are presented in Figures 2, 4, 6 and 8, respectively.

The X-ray structural study of **2** reveals a highly distorted octahedral geometry with the thiocyanato ligands *cis* to each other and a folded conformation of the L^{B5} tetradentate ligand (Figure 2). This strong deviation of the coordination site from the regular octahedron, suggested by the Fe–N distances and N–Fe–N angles, is associated with the HS electronic configuration.

The crystal packing of **2** is characterized by isolated dimeric units (Figure 3) formed through π–π stacking interactions between centrosymmetrically related $[FeL^{B5}(NCS)_2]$ molecules ($1-x$, $2-y$, $2-z$) with a centroid-to-centroid distance of 3.50 Å. Other intermolecular separations equal or exceed the sum of van der Waal radii.

The Fe^{2+} ion in complex **3** (Figure 4) presents a slightly distorted N_6 octahedral environment constituted by four nitrogen atoms from the L^{E1} tetradentate ligand (two N_{imino}, one $N_{pyridyl}$ and one $N_{imidazolyl}$) and two N donors from the *trans*-coordinated NCS^- anions. The values of the Fe–N bond lengths are in the range 1.932–2.028 Å, and they are indicative of a LS state of Fe^{II} in complex **3** at 180 K.

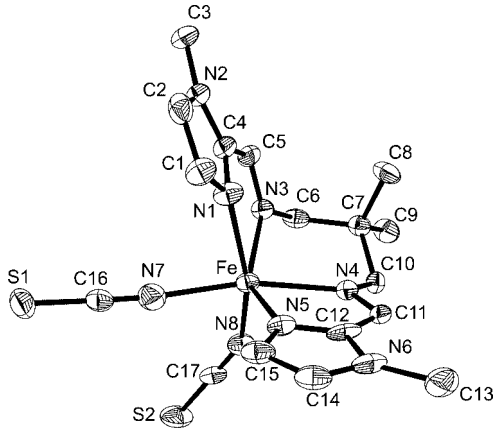

Figure 2. Molecular structure of $[FeL^{B5}(NCS)_2]$ (**2**). Thermal ellipsoids are drawn at the 40% probability level. H atoms have been omitted for clarity. Selected bond lengths [Å] and angles [°]: Fe–N1 2.235(4), Fe–N3 2.185(4), Fe–N4 2.212(7), Fe–N5 2.144(5), Fe–N7 2.122(10), Fe–N8 2.119(5); N1–Fe–N3 73.49(16), N1–Fe–N4 107.9(2), N1–Fe–N5 87.79(18), N1–Fe–N7 81.7(3), N1–Fe–N8 158.2(2), N3–Fe–N4 79.8(2), N3–Fe–N5 142.8(3), N3–Fe–N7 112.1(2), N3–Fe–N8 93.15(16), N4–Fe–N5 75.8(3), N4–Fe–N7 166.86(16), N4–Fe–N8 85.9(2), N5–Fe–N7 96.0(3), N5–Fe–N8 112.37(16), N7–Fe–N8 87.9(3).

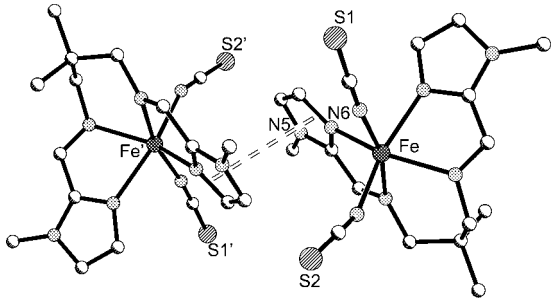

Figure 3. π–π stacking interactions in the crystal structure of $[FeL^{B5}(NCS)_2]$ (**2**).

Both H-bonds and π–π stacking interactions are responsible for the crystal packing of **3**. $[FeL^{E1}(NCS)_2]$ molecules are alternately associated into infinite chains through two N–H···S hydrogen bonds with the following parameters: N2···S1′ (x, $1-y$, $1+z$) = 3.330(2) Å, N2–H = 0.86 Å, ∠N2–H···S1′ = 160.0°. Interactions of the π–π type be-

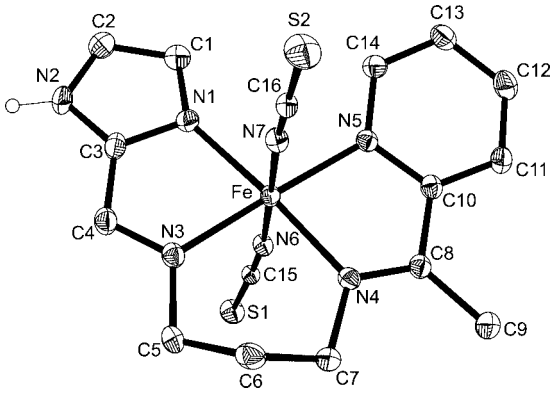

Figure 4. Molecular structure of $[FeL^{E1}(NCS)_2]$ (**3**). Thermal ellipsoids are drawn at the 40% probability level. H atoms have been omitted for clarity. Selected bond lengths [Å] and angles [°]: Fe–N1 2.0277(17), Fe–N3 1.9618(17), Fe–N4 1.9493(17), Fe–N5 1.9692(17), Fe–N6 1.9391(18), Fe–N7 1.9324(18); N1–Fe–N3 80.67(7), N1–Fe–N4 174.76(7), N1–Fe–N5 101.71(7), N1–Fe–N6 87.95(7), N1–Fe–N7 91.52(7), N3–Fe–N4 96.80(7), N3–Fe–N5 177.25(7), N3–Fe–N6 88.82(7), N3–Fe–N7 90.45(7), N4–Fe–N5 80.94(7), N4–Fe–N6 87.41(7), N4–Fe–N7 93.09(7), N5–Fe–N6 92.62(7), N5–Fe–N7 88.13(7), N6–Fe–N7 179.15(7).

tween centrosymmetrically related $(1-x, -y, 1+z)$ pyridine rings with a centroid-to-centroid distance of 3.62 Å organize the chains into 2D layers, a fragment of which is shown in Figure 5.

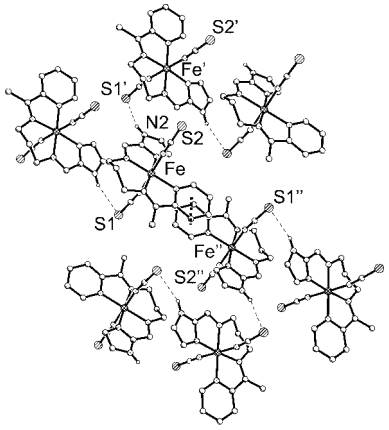

Figure 5. Fragment of a 2D layer of $[FeL^{E1}(NCS)_2]$ (**3**) that shows the H-bonds and π–π stacking interactions responsible for the crystal packing.

Solution and further refinement of the crystal structure of complex **5**, $[FeL^{E3}(NCS)_2]$, showed the presence of a statistical disorder of the external parts of the ligand. As a result, L^{E3} occupies two distinct positions around Fe (Figure 6), related by C2 rotation through the Fe···C6 axis. The refined values of the site occupancy factors are equal to 0.74 and 0.26 for the major and minor (*) components, respectively. The average value of the Fe–N bond lengths, 1.969 Å, evidences the LS state of Fe^{II} in **5** at 180 K.

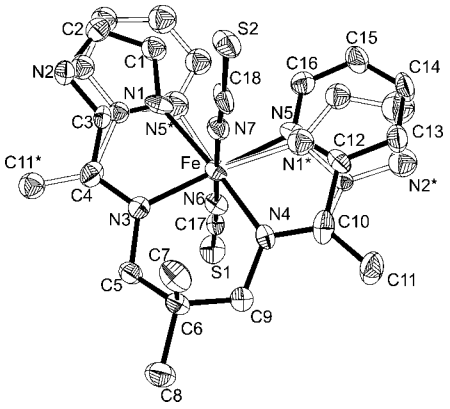

Figure 6. Molecular structure of $[FeL^{E3}(NCS)_2]$ (**5**). Thermal ellipsoids are drawn at the 40% probability level. H-atoms have been omitted for clarity. The minor location of L^{E3} is drawn with thin lines. Selected bond lengths [Å] and angles [°]: Fe–N1 2.061(6), Fe–N1* 2.028(14), Fe–N3 1.946(4), Fe–N4, 1.939(4), Fe–N5 1.962(6), Fe–N5* 1.957(13), Fe–N6 1.928(4), Fe–N7 1.931(4); N1–Fe–N3 78.6(2), N1*–Fe–N3 171.7(7), N1–Fe–N4 173.0(3), N1*–Fe–N4 76.1(7), N1–Fe–N5 102.1(4), N1*–Fe–N5* 99.8(8), N1–Fe–N6 93.4(2), N1*–Fe–N6 90.8(8), N1–Fe–N7 85.2(2), N1*–Fe–N7 87.1(8), N3–Fe–N4 95.65(15), N3–Fe–N5 177.5(3), N3–Fe1–N5* 88.5(5), N3–Fe–N6 90.17(15), N3–Fe–N7 92.17(15), N4–Fe–N5 83.5(3), N4–Fe–N5* 174.6(5), N4–Fe–N6 90.56(16), N4–Fe–N7 91.11(15), N5–Fe–N6 92.1(3), N5*–Fe–N6 86.0(5), N5–Fe–N7 85.6(3), N5*–Fe–N7 92.2(5), N6–Fe–N7 176.98(16).

The crystal packing of **5** is essentially determined by the only possible N–H···S hydrogen bond [N2H···S2′ $(1+x, y, z)$ = 3.37 Å, H(N2)···S2′ = 2.52(4) Å, ∠N2HS2′ = 168.5°], which leads to the formation of infinite chains, as depicted in Figure 7. Further association of the components occurs through the short S2···S1′$(x-0.5, 0.5-y, 0.5+z)$ interchain contacts (3.38 Å), which result in 2D layers parallel to the [010] plane.

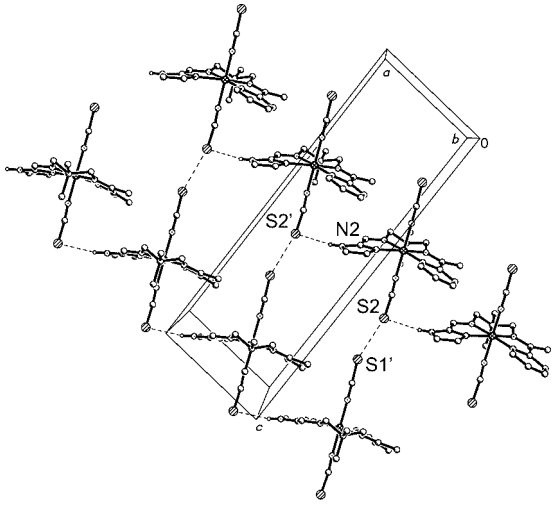

Figure 7. Fragment of a 1D chain of $[FeL^{E3}(NCS)_2]$ **5** that shows the H-bonds responsible for the crystal packing.

Complex **6** has a molecular structure that consists of neutral $[FeL^{E4}(NCS)_2]$ complex molecules as depicted in Figure 8. Geometrical parameters (Fe–N distances and N–

Fe–N angles) of the Fe $–N_6$ core at 180 K, close to those of a regular octahedron, indicate a LS electronic configuration of the Fe^{2+} ions.

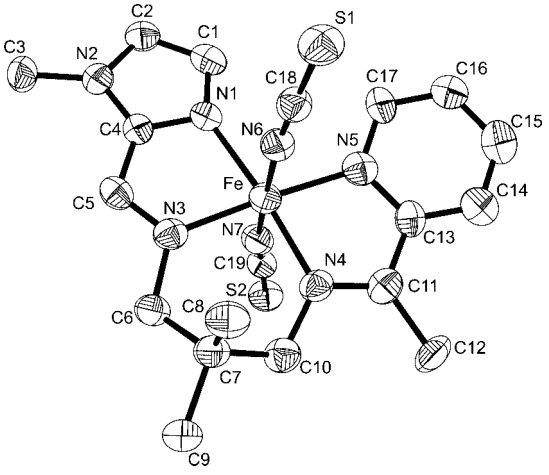

Figure 8. Molecular structure of $[FeL^{E4}(NCS)_2]$, the complex molecule of **6**. Thermal ellipsoids are drawn at the 40% probability level. H-atoms have been omitted for clarity. Selected bond lengths [Å] and angles [°]: Fe–N1 2.048(6), Fe–N3 1.945(6), Fe–N4 1.948(6), Fe–N5 1.946(7), Fe–N6 1.948(7), Fe–N7 1.944(7); N1–Fe–N3 81.4(3), N1–Fe–N4 174.0(2), N1–Fe–N5 102.7(3), N1–Fe–N6 88.0(3), N1–Fe–N7 89.6(3), N3–Fe–N4 94.8(3), N3–Fe–N5 175.8(3), N3–Fe–N6 92.0(3), N3–Fe–N7 91.6(3), N4–Fe–N5 81.2(3), N4–Fe–N6 96.8(3), N4–Fe–N7 85.8(3), N5–Fe–N6 87.1(3), N5–Fe–N7 89.5(3), N6–Fe–N7 175.3(3).

MeOH solvate molecules are associated to the $[FeL^{E4}(NCS)_2]$ complex molecules in the 1:1 ratio through O–H···S hydrogen bonds with distances O1–H = 1.03 Å, O1···S2 = 3.227(7) Å and O1–H···S2 = 2.30 Å and ∠O1HS2 = 149.9° (Figure 9). In addition, π–π stacking interactions between centrosymmetrically related ($–x$, $2–y$, $1–z$) imidazolyl rings are evidenced by the short interplanar (3.49 Å) and centroid-to-centroid (3.88 Å) distances. Centrosymmetric $\{[FeL^{E4}(NCS)_2]\cdot CH_3OH\}_2$ pairs are quite separated in the crystal space as a result of this π–π stacking interaction. In this respect, the crystal packing motif of **6** resembles that of **2**.

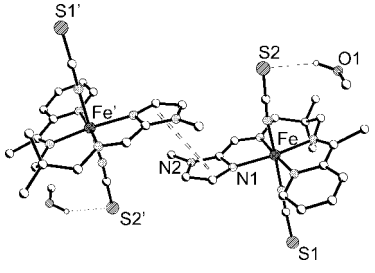

Figure 9. The dimeric association in $[FeL^{E4}(NCS)_2]\cdot CH_3OH$ (**6**) that shows the H-bonds and π–π stacking interactions responsible for the crystal packing.

Magnetic Studies

The thermal variation of the magnetic susceptibility χ_M was explored for complexes **1** and **3**–**6**: the $\chi_M T$ data for selected temperatures (T) are collated in Table S1 (Supporting Information). The $\chi_M T$ vs. T data are shown in Figure 10 for complexes **1** and **3**–**6**. It was not possible to study the magnetic properties of **2**, because this sample was obtained in very poor yield as a mixture with complex **6** (see Experimental Section).

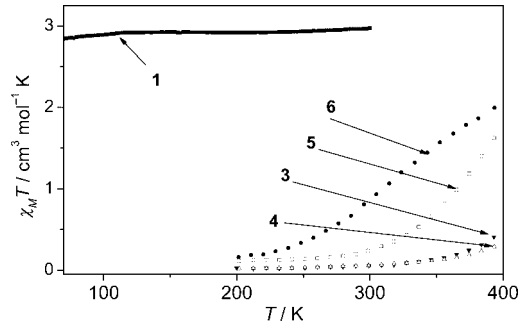

Figure 10. Thermal variation of the $\chi_M T$ product for complexes **1** and **3**–**6**.

The magnetic study of **1** shows that this complex is in the HS state between 70 and 300 K, with a $\chi_M T$ value close to 3 $cm^3 mol^{-1} K$. The $\chi_M T$ product for complexes $[FeL^{E1}(NCS)_2]$ (**3**; R^1 = H, R^2 = H) and $[FeL^{E2}(NCS)_2]$ (**4**; R^1 = H, R^2 = Me) is practically constant over the 200–350 K range and characteristic of LS Fe^{II} $\chi_M T \approx 0$ $cm^3 mol^{-1} K$). The slight increase in $\chi_M T$ above 350 K ($\chi_M T$ = 0.4 $cm^3 mol^{-1} K$ at 400 K) may be considered as the onset of SC, with ca. 10% of HS sites at 400 K. Similarly, the $\chi_M T$ product for **5** (R^1 = Me, R^2 = H) is practically constant from 200 to 300 K and characteristic of LS Fe^{II}. Then, $\chi_M T$ increases from 0.2 $cm^3 mol^{-1} K$ at 300 K to 1.6 $cm^3 mol^{-1} K$ at 400 K, indicating LS→HS SC of ca. 50% Fe^{II} centres at 400 K. Complex **6** (R^1 = Me, R^2 = Me) is essentially LS at 200 K ($\chi_M T$ = 0.4 $cm^3 mol^{-1} K$) and exhibits a smooth and incomplete SC upon heating with ca. 60% Fe^{II} sites in the HS state at 400 K. Relative to that of complex **5**, the SC is smoother for **6**. The same behaviour is observed in the cooling mode, indicating the absence of hysteresis for these compounds.

Mössbauer Spectroscopy

$[FeL^{Bx}(NCS)_2]$ Complexes

Mössbauer spectra were recorded at selected temperatures in the 80–250 K range for complexes **1** and **2**. Values of the Mössbauer parameters (isomer shift δ, quadrupole splitting ΔE_Q and line width $\Gamma/2$) resulting from fitting the spectra are collated in Table S2 (Supporting Information). The isomer shift values decrease slightly with increasing temperature, indicating the operation of second-order Doppler effect.[5]

The Mössbauer spectra of **1** evidence two HS doublets characteristic of slightly inequivalent Fe centres, Fe^{II}(A) and Fe^{II}(B) sites, as previously observed in related complexes.[4a] These doublets were fitted with similar isomer shift

values [1.098(2) and 1.120(2) mm s^{-1} at 80 K, Table S2] as expected for identical N_6 donor sets around Fe^{II}(A) and Fe^{II}(B) and different ΔE_Q values [2.582(8) and 2.982(8) mm s^{-1} at 80 K for Fe^{II}(A) and Fe^{II}(B), respectively], suggesting different low symmetry environments (Figure 11).[5]

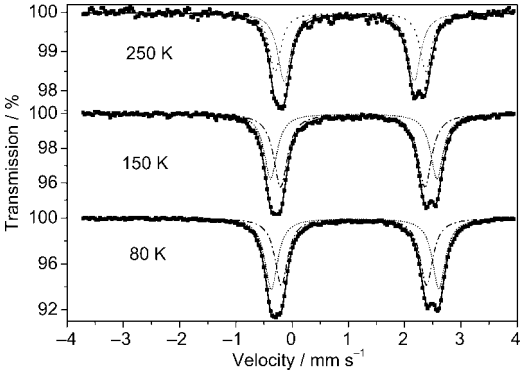

Figure 11. Representative least-squares-fitted Mössbauer spectra of [FeL^{B4}(NCS)$_2$] **1**. The solid line represents the fit of the data to two subspectra, the dash–dot line corresponds to site A and the dotted line to site B with the parameters given in the text and in Table S2.

In contrast, **2** is characterized by a unique quadrupole-split doublet [δ = 1.17(2) and ΔE_Q = 2.66(4) mm s^{-1} at 80 K] typical of HS iron(II). The Mössbauer spectra of **2** were obtained from a sample resulting from the synthetic procedure described in the Experimental Section of **6**: this sample was the first solid obtained, specifically a mixture of **2** (red crystals) and **6** (dark-blue powder), because it was not possible to isolate enough red crystals of **2** in order to carry out Mössbauer measurements. The second solid (pure single crystals of **6**) were obtained in good yield through slow evaporation of the resulting filtrate; it was then possible to carry out Mössbauer measurements of **6** (pure) and thus to ascertain that the major doublet in the Mössbauer spectrum of the mixture was indeed that of **6**, and moreover to evaluate the relative ratio of **2** [11(2)%] in its mixture with **6**.

[FeL^{Ex}(NCS)$_2$] Complexes

The Mössbauer spectra of complexes **3**–**6** confirm the spin states deduced from the magnetic data for these materials (Table S2, Supporting Information); however, as a result of poor counting statistics, high-temperature spectra (350–400 K) of complexes **3**, **4** and **5** could not be obtained in good quality. As an example for the materials in this series, we describe the study of complex **6** for which representative Mössbauer spectra recorded in the heating mode are shown in Figure 12. These spectra, measured in the 200–400 K range, confirm the partial SC deduced from the magnetic measurements. At 200 K, a unique LS doublet [δ = 0.417(4) and ΔE_Q = 0.787(8) mm s^{-1}] is observed;[4–7] at and above 300 K, the asymmetry of this doublet results from the presence of a growing HS component that is difficult to fit owing to the poor counting statistics. This Mössbauer behaviour confirms the SC observed by magnetic measurements. It is also worth mentioning that these high temperature spectra are very broad [$\Gamma_{1/2}$(LS) = 0.22 mm s^{-1}, $\Gamma_{1/2}$(HS) = 0.23 mm s^{-1}]. In the case of SC materials, observation of broadened Mössbauer spectra is usually related to dynamic phenomena: the interstate conversion rates K_{LH} (LS→HS) and K_{HL} (HS→LS) are comparable to the hyperfine frequency (10^8 s^{-1}).[8,9]

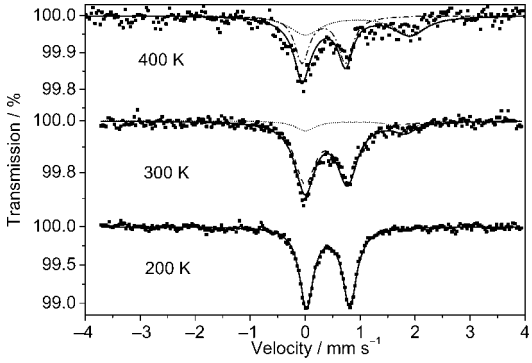

Figure 12. Representative least-squares-fitted Mössbauer spectra of [FeL^{E4}(NCS)$_2$] (**6**). The solid line represents the fit of the data to two subspectra, the dash–dot line corresponds to the LS site and the dotted line to the HS site with the parameters given in the text and in Table S2.

Mössbauer spectra of complexes **3**, **4** and **5** were recorded between 77 and 300 K. In agreement with the magnetic studies, all spectra show a unique doublet with parameters characteristic of the LS iron(II) state [δ = 0.376(1), ΔE_Q = 0.719(2) mm s^{-1} for **3** at 293 K; δ = 0.357(4), ΔE_Q = 0.663(7) mm s^{-1} for **4** at 293 K; δ = 0.377(4), ΔE_Q = 0.634(8) mm s^{-1} for **5** at 300 K; Table S2).

IR Spectroscopy

The IR spectroscopic study was focused on the NCS stretching absorptions (2000–2100 cm^{-1} range), which serves as a good sensor for the *cis* or *trans* conformation of the coordinated thiocyanate anions. Usually, *trans* isomers exhibit a single absorption, whereas *cis* isomers are characterized by a splitting of the ν_{CN} absorption.[10] However, this criterion must be considered with much caution because the splitting of this band is very sensitive to slight deformations of the coordination sphere (in particular the N–M–N angle between the two thiocyanate ligands coordinated to the metal centre). The IR spectrum of [FeL^{B4}(NCS)$_2$] (**1**) shows two doublets (2081, 2070 and 2052, 2036 cm^{-1}), and this is similar to that of [FeL^{B1}(NCS)$_2$],[4a] which shows one doublet (2097, 2095 cm^{-1}) and one singlet (2025 cm^{-1}; Figure S1). The X-ray structure of [FeL^{B1}(NCS)$_2$] evidences two independent *trans* NCS molecules with strongly and differently distorted octahedral symmetries and its Mössbauer spectra confirm the presence of two HS Fe^{II} sites.[4a] The presence of two HS Fe^{II} sites {with δ and ΔE_Q parameters similar to those of [FeL^{B1}(NCS)$_2$]} in the Mössbauer spectra of **1**, together with the similarity of its IR spectrum to that of [FeL^{B1}(NCS)$_2$], strongly advocates to the similarity of their molecular structures with two independent *trans* NCS molecules with strongly and differently distorted octahedral

symmetry. As mentioned above, the splitting (or broadening) of the ν_{CN} absorptions is characteristic of a strong distortion of the octahedral symmetry. In contrast, the X-ray structure of $[FeL^{B2}(NCS)_2]$ evidences only one *trans* molecule with strongly distorted octahedral symmetry and the Mössbauer spectra of $[FeL^{B2}(NCS)_2]$ and $[FeL^{B3}(NCS)_2]$ show the presence of one HS Fe^{II} site.[4a] The IR spectra of $[FeL^{B2}(NCS)_2]$ and $[FeL^{B3}(NCS)_2]$ show one doublet (2093, 2065 and 2082, 2018 cm^{-1}, respectively; Figure S1), and they are in agreement with the strong distortion of their unique *trans* NCS molecule. Consequently, the four bands between 2081 and 2036 cm^{-1} observed for **1** confirm the presence of two distinct *trans* isomers as observed through Mössbauer spectroscopy, and in accordance with previous studies.[4]

Discussion

As part of our systematic approach to generate new ferrous materials of the general formula $[FeL(NCS)_2]$ with predictable magnetic properties, in this contribution we report the results obtained when 1-*N*-R^2-imidazole-2-carboxaldehyde (R^2 = H, Me) is used as a carbonyl synthon in combination with 1,3-diaminopropane and 2,2-dimethyl-1,3-diaminopropane as diamino synthons for the synthesis of symmetrical L^{Bx} and dissymmetrical L^{Ex} tetradentate Schiff base ligands (Figures 1 and 13).

The change in carbonyl synthon from 2-R^2-imidazole-4-carboxaldehyde (R^2 = H, CH_3, C_6H_5)[4a] or 5-methylimidazole-4-carboxaldehyde[4b] to 1-*N*-R^2-imidazole-2-carboxaldehyde (R^2 = H, CH_3) involves minor structural modifications in the case of $[FeL^{B4}(NCS)_2]$ (**1**; R^2 = H), which is characterized by a *trans* coordination of the thiocyanato ligands and a planar conformation of L^{B4}, as suggested by comparison of the IR spectra and X-ray data of $[FeL^{B1}(NCS)_2]$, $[FeL^{B2}(NCS)_2]$ and **1**. These three complexes have the same coordination sphere and a very similar geometry around the metal centre with a planar conformation of L^{Bx} (see above and ref.[4a]). However, in $[FeL^{B5}(NCS)_2]$ (**2**; R^2 = CH_3), which is characterized by a *cis* coordination of the thiocyanato ligands, L^{B5} has a folded conformation, as demonstrated by X-ray analysis (see above). One plausible explanation for obtaining different isomers is the absence/presence of a methyl substituent at the 1-*N*-imidazole, which would allow/prevent the involvement of N–H hydrogen bonds as observed in the previous studies[4a,4b] and also for $[FeL^{Ex}(NCS)_2]$ complexes described in the present report. In the crystal structure of **2**, the *cis* arrangement of the thiocyanato anions associated to the folded conformation of the tetradentate ligand allows π–π stacking interactions between adjacent imidazolyl rings, which result in a crystal packing made of isolated dimeric associates. Although no structural data is available for **1**, the *trans* NCS coordination is likely to be promoted by N–H···S and/or N–H···N hydrogen bonds as observed in $[FeL^{B1}(NCS)_2]$,[4a] $[FeL^{B2}(NCS)_2]$,[4a] $[FeL^{D2}(NCS)_2]$,[4b] **3** and **5** (this work).

With regard to the series based on the disymmetrical L^{Ex} ligands, we may establish a parallelism between the statistical disorder of L^{E3} observed in **5**, which implies the presence of two configurations of the propylene fragment and the statistical disorder of the propylene fragment of L^{D2} in $[FeL^{D2}(NCS)_2]$ at and below 300 K.[4b] Two conformers similarly distinguished by the configuration of one of the propylene fragments of H_2L^{2-Me} were also observed in the crystal structure of $[FeH_2L^{2-Me}](ClO_4)_2$ (H_2L^{2-Me} = bis{[(2-methylimidazol-4-yl)methylidene]-3-aminopropyl}ethylene diamine) at low temperature.[2k] Although no molecular structure is available, it is thus likely that the two-step SC of $[FeL^{D1}(NCS)_2]$, which is also characterized by two quadrupole-split LS doublets at low temperature,[4b] originates from the presence of two conformers distinguished by the configuration of the propylene fragment of L^{D1}.

Similar to the previously reported $[FeL^{Cx}(NCS)_2]$[4a] and $[FeL^{Dx}(NCS)_2]$[4b] series (Figure 14), the electronic behaviours of **3**–**6** evidences that a combination of pyridyl and imidazolyl rings to yield Fe^{II} complexes that are based on a dissymmetrical tetradentate L^{Ex} ligand allows the generation of an intermediate ligand field suitable for SC. In the absence of substituents on the central carbon atom of the propylene bridge of L^{Ex} (R^1 = H, **3** and **4**), the onset of SC is above 350 K, regardless of the 1-*N*-R^2-imidazolyl substit-

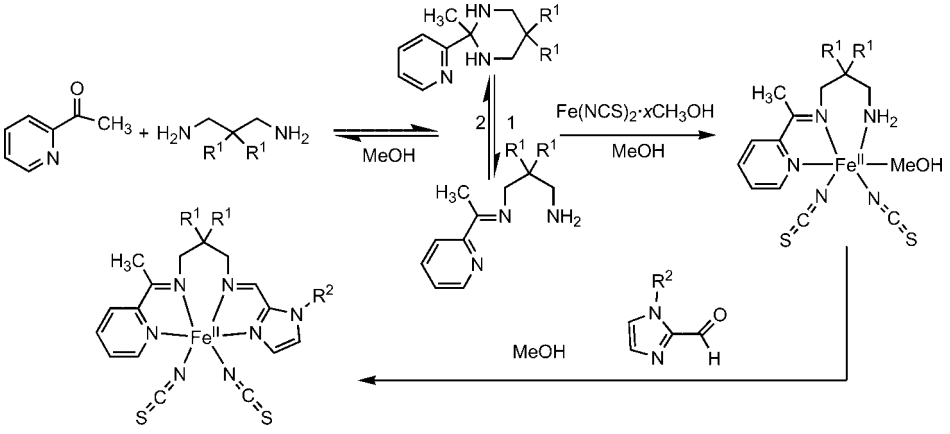

Figure 13. Synthetic pathway for the $[FeL^{Ex}(NCS)_2]$ (R^1 = H, Me; R^2 = H, Me).

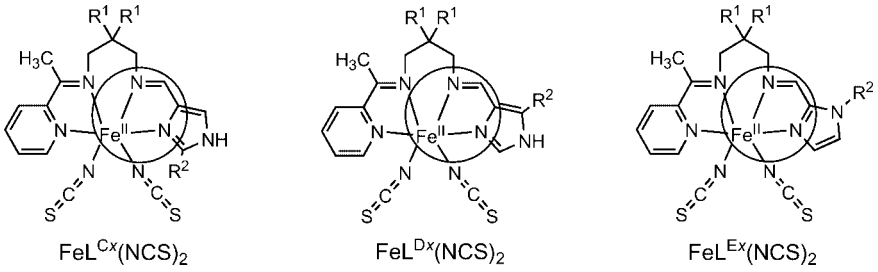

Figure 14. Compared schematic drawings of the $[FeL^{Cx}(NCS)_2]$,[4a] $[FeL^{Dx}(NCS)_2]$[4b] and $[FeL^{Ex}(NCS)_2]$ complexes (this work).

uent. Because the electronic properties of these materials cannot be evaluated above ca. 400 K, the effect of the 1-*N*-R^2-imidazolyl substituent on the compared SC behaviours of **3** and **4** cannot be appreciated. In the presence of substituents on the central carbon atom of the propylene bridge of L^{Ex} (R^1 = Me, **5** and **6**), the SC is shifted towards lower temperatures. This down shift is modulated by the effect of the 1-*N*-R^2-imidazolyl substituent in two ways: (1) $T_{1/2}$ is higher for **5** (R^2 = H) than for **6** (R^2 = Me), ca. 390 vs. ca. 360 K and (2) the SC is much steeper for **5** than for **6**, indicating a more cooperative behaviour of **5** in line with the presence of extended intermolecular interactions in **5** versus isolated dimeric associates in **6**. The higher $T_{1/2}$ for **5** (R^2 = H) relative to that of **6** (R^2 = Me) is in line with our previous studies showing that the ligand fields exerted by L^{C1} and L^{C4} (R^2 = H) are weaker (higher $T_{1/2}$) than those exerted by the remaining L^{Cx} ligands (R^2 = Me or Ph).[4a] However, the R^2 substituent is at the C2 imidazolyl in the L^{Cx} series, whereas it is at the 1-*N*-imidazolyl in the present L^{Ex} series (Figure 14); thus both the steric and inductive effects of R^2 are significantly different from one series to the other one, which prevents a more detailed comparison.

From our previous studies,[4a,4b] the role of R^1 in tuning the ligand field, as estimated through approximated $T_{1/2}$ values, was considered as more limited than that of R^2 and opposite in trend (lower $T_{1/2}$ associated with R^1 = H). It may thus seem striking to observe the opposite situation for the present series where the role of R^1 in tuning the ligand field is larger than (and similar in trend to) that of R^2. However, it must be underlined that the change in carbonyl synthon from 2-R^2-imidazole-4-carboxaldehyde[4a] or 5-methylimidazole-4-carboxaldehyde[4b] to 1-*N*-R^2-imidazole-2-carboxaldehyde (this work) moves the connection of the imidazolyl fragment (to the propyl chain) from the 4- to the 2-imidazolyl position: this change switches the orientation of the coordinated imidazolyl and the position of the imine imidazolyl nitrogen with respect to the adjacent Schiff base imine function (Figure 14). As a result, in the present $[FeL^{Ex}(NCS)_2]$ series the metallacycle involving the imidazolyl fragment is highly conjugated (Fe–N=C–C=N–) at variance with the corresponding metallacycle in the $[FeL^{Cx}(NCS)_2]$[4a] and $[FeL^{Dx}(NCS)_2]$[4b] series (Fe–N–C–C=N–), see Figure 14. It is then clear that this electronic effect not only largely overpasses but also qualitatively and quantitatively modifies the effects of R^1 and R^2.

As a final comment, we would like to stress the role of hydrogen bonds in the SC behaviour within this series of compounds: involvement of 1-*N*-Me-imidazole-2-carboxaldehyde for the synthesis of dissymmetrical ligands **4** and **6** prevents $NH_{imidazole}$···SCN interactions. Indeed, no weak interactions of this type are found in **6**, yielding isolated dimeric associates through π–π stacking interactions. As a consequence, **6** exhibits a very smooth SC that spreads over 200 K because of the lack of intermolecular interactions/cooperativity relative to its chemical isomer $[FeL^{D1}(NCS)_2]$ (including the 5-methyl-4-imidazolyl fragment), which exhibits a steep SC with a 5 K hysteresis.[4b]

Experimental Section

General: All reagents and solvents are commercially available (Aldrich, Wako), and they were used without further purification. Elemental analyses were carried with a Perkin–Elmer 2400 series II device (C, H, N) at the Microanalytical Laboratory of the Laboratoire de Chimie de Coordination in Toulouse, and with a Maxim Thermoelectron device (S, Fe) at the Service Central de Microanalyses du CNRS in Vernaison, France. 1D ^{1}H and 1D ^{13}C NMR spectra were obtained with an AC 250 FT spectrometer (Bruker). Chemical shifts are given relative to tetramethylsilane by using $CDCl_3$ as the solvent. IR spectra were measured in the 400–4000 cm^{-1} range with a 9800 FTIR spectrometer (Perkin–Elmer). Mössbauer spectra were recorded with a constant-acceleration conventional spectrometer with a 50 mCi source of ^{57}Co (Rh matrix). The absorber was a powdered sample enclosed in a 20-mm diameter cylindrical plastic sample holder, the size of which was determined to optimize the absorption. Spectra were obtained in the 80–400 K range by using a MD306 Oxford cryostat (4–293 K) or an homemade vacuum oven (300–500 K), the thermal scanning being monitored by an Oxford ITC4 servo control device (± 0.1 K accuracy). A least square computer program[12] was used to fit the Mössbauer parameters and to determine their standard deviations of statistical origin (given in parentheses). Isomer shift values (δ) are relative to iron foil at 293 K. Variable temperature magnetic susceptibility data were collected from powdered samples with a MPMS-55 Quantum design SQUID magnetometer or a Faraday type susceptometer under applied magnetic fields lower than 0.5 T. Diamagnetic corrections were applied by using Pascal's constants.[13]

Synthesis of Ligands

Symmetrical Ligands L^{Bx}: 2,2-Dimethyl-1,3-diaminopropane (0.102 g, 10^{-3} mol) and imidazole-2-carboxaldehyde (0.192 g,

2×10^{-3} mol, for L^{B4}) or 1-methylimidazole-2-carboxaldehyde (0.220 g, 2×10^{-3} mol, for L^{B5}) in methanol (20 mL) were stirred for 2 h at r.t. Slow evaporation of the solvent yielded brown-yellow oils. Yield: 0.190 g (74%) and 0.234 g (82%) for L^{B4} and L^{B5}, respectively. Data for L^{B4}: ^{1}H NMR (250 MHz, $CDCl_3$): δ = 8.16 (s, 2 H, 4-H), 7.14 (s, 2 H + 2 H, 1-H + 2-H, NH proton exchange did not allow distinguishing the two types of protons), 3.43 (s, 4 H, 5-H5), 0.90 (s, 6 H, 7-H) ppm. Data for L^{B5}: ^{1}H NMR (250 MHz, $CDCl_3$): δ = 8.26 (s, 2 H, 4-H), 7.05–6.88 (2s, 2 H + 2 H, 1-H + 2-H), 3.956 (s, 6 H, 3-H), 3.42 (s, 4 H, 5-H), 0.97 (s, 6 H, 7-H).

Synthesis of the Half-Units L and L′: The synthetic pathway was adapted from ref.[4b]: 2-acetylpyridine and 1,3-diaminopropane (for L) or 2,2-dimethyl-1,3-diaminopropane (for L′) were mixed for 30 min in a 1:1 ratio (1 equiv. = 10^{-3} mol) in methanol (10 mL). The resulting pale yellow solution was used immediately for the preparation of complexes **3**–**6**.

Synthesis of Complexes

All complexation reactions and sample preparations for physical measurements were carried out under a purified nitrogen atmosphere within a glove box (Vacuum Atmospheres H.E.43.2) equipped with a dry train (Jahan EVAC 7).

$Fe(NCS)_2 \cdot x$MeOH: Prepared through the 1:2 reaction of $Fe(ClO_4)_2 \cdot xH_2O$ with potassium thiocyanate in MeOH.[11] After removal of potassium perchlorate through filtration, the freshly prepared $Fe(NCS)_2 \cdot x$MeOH was used immediately for the preparation of complexes **1**–**6**.

Caution: Although no such behaviour was observed during the present work, perchlorate salts are potentially explosive and should be handled in small quantities and with much care.

General Procedure for 1 and 2: A methanolic solution (10^{-3} mol in 10 mL) of $[Fe(NCS)_2] \cdot x$MeOH was added slowly to a methanolic solution (10^{-3} mol in 10 mL) of the ligand. The solution immediately changed from pale yellow to orange-yellow and was stirred for 30 min.

$[FeL^{B4}(NCS)_2]$ (1): Yield: 0.28 g, 65%, microcrystalline powder. IR: 2081, 2070, 2052, 2036 (NCS, 4 bands), 1619 (imine) cm^{-1}. $C_{15}H_{18}FeN_8S_2$ (430.3): calcd. C 41.87, H 4.22, N 26.04, S 14.90, Fe 12.98; found C 41.68, H 3.91, N 25.36, S 14.23, Fe 12.67.

$[FeL^{B5}(NCS)_2]$ (2): Could not be obtained as a pure species through the general method described above. However, during the synthesis of **6** with the dissymmetrical ligand L^{E4}, see below, we observed the systematic (and reproducible) formation of single crystals of red complex **2** in a poor yield, mixed with the desired dark-blue complex **6**. The amount of **2** in this mixture was evaluated by Mössbauer spectroscopy to 11(2)% (Table S2). The red single-crystal selected for X-ray data collection was picked from the mixture of **2** and **6**, see synthetic details for **6**, below.

General Procedure for 3–6: The synthetic pathway was adapted from the method previously described[4] (Figure 13). To a pale-yellow solution (10^{-3} mol, 10 mL of methanol) of aminal L, **3** or **4**, or L′, **5** or **6**, was slowly added the freshly prepared $Fe(NCS)_2$ solution (10^{-3} mol, 10 mL of methanol). The colour of the reaction mixture immediately turned to dark blue, and the mixture was stirred for 5 min. The appropriate 1-*N*-R^1-imidazole-2-carboxaldehyde (10^{-3} mol, 10 mL of methanol) was then added (imidazole-2-carboxaldehyde for **3** and **5**, and 1-*N*-methyl-imidazole-2-carboxaldehyde for **4** and **6**). No further colour change was observed; the solution was stirred for another 30 min and then left undisturbed until a microcrystalline powder or crystals formed quantitatively.

$[FeL^{E1}(NCS)_2]$ (3): Yield: 0.32 g, 75%, dark-blue single crystals. IR (KBr): 2125, 2113 (NCS); 1645 (imine) cm^{-1}. $C_{16}H_{17}FeN_7S_2$ (427.3): calcd. C 44.97, H 4.01, N 22.94, S 15.01, Fe 13.07; found C 45.29, H 3.72, N 22.75, S 14.68, Fe 12.72.

$[FeL^{E2}(NCS)_2]$ (4): Yield: 0.32 g, 73%, dark-blue microcrystalline powder. IR (KBr): 2109, 2080 (NCS), 1647 (imine) cm^{-1}. $C_{17}H_{19}FeN_7S_2$ (441.4): calcd. C 46.26, H 4.34, N 22.22, S 14.53, Fe 12.65; found C 46.15, H 4.18, N 21.86, S 13.96, Fe 11.96.

$[FeL^{E3}(NCS)_2]$ (5): Yield: 0.31 g, 68%, dark-blue single crystals. IR (KBr): 2127, 2111 (NCS), 1656 (imine) cm^{-1}. $C_{18}H_{21}FeN_7S_2$ (455.4): calcd. C 47.48, H 4.65, N 21.53, S 14.08, Fe 12.26; found C 48.02, H 4.43, N 21.34, S 13.68, Fe 11.88.

$[FeL^{E4}(NCS)_2] \cdot CH_3OH$ (6): After removal of a small amount of a mixture of **2** and **6** by filtration, **6** was obtained from the resulting filtrate 2 d later. Yield: 0.36 g, 72%, dark-blue single crystals. IR (KBr): 2113, 2070 (NCS), 1635 (imine) cm^{-1}. $C_{20}H_{27}FeN_7OS_2$ (501.4): calcd. C 47.91, H 5.42, N 19.55, S 12.79, Fe 11.14; found C 47.69, H 4.92, N 20.13, S 12.43, Fe 10.86.

Table 1. Crystallographic data collection and structure determination for complexes **2**, **3**, **5** and **6**.

Compound	$[FeL^{B5}(NCS)_2]$ (**2**)	$[FeL^{E1}(NCS)_2]$ (**3**)	$[FeL^{E3}(NCS)_2]$ (**5**)	$[FeL^{E4}(NCS)_2]$ CH_3OH (**6**)
Formula	$C_{17}H_{22}FeN_8S_2$	$C_{16}H_{17}FeN_7S_2$	$C_{18}H_{21}FeN_7S_2$	$C_{20}H_{27}FeN_7OS_2$
Formula weight	458.40	427.34	455.39	501.43
Crystal system	monoclinic	monoclinic	monoclinic	monoclinic
Space group	$P2_1/n$	$P2_1/c$	$P2_1/n$	$P2_1/c$
a / Å	9.966(2)	8.8108(5)	8.114(3)	8.1657(11)
b / Å	8.4072(17)	24.3767(14)	11.208(5)	19.007(2)
c / Å	25.953(5)	8.6855(5)	23.067(19)	15.3398(19)
α / °	90	90	90	90
β / °	93.61(3)	90.076(5)	95.83(4)	100.787(15)
γ / °	90	90	90	90
V / Å^3	2170.2(8)	1865.45(18)	2087(2)	2338.7(5)
Z	4	4	4	4
$\rho_{calcd.}$ / g cm^{-3}	1.403	1.522	1.449	1.416
λ / Å	0.71073	0.71073	0.71073	0.71073
T / K	180	180	180	180
μ(Mo-K_α) / cm^{-1}	0.907	1.048	0.941	0.850
R[a] [$I > 2\sigma(I)$]	0.0600	0.0327	0.0579	0.0845
wR[b]	0.1219	0.0846	0.1232	0.1887

[a] $R = \Sigma F_o - F_c / \Sigma F_o$. [b] $wR = [\Sigma w(F_o^2 - F_c^2)^2 / \Sigma w F_o^{22}]^{1/2}$.

Crystallographic Data Collection and Structure Determination for 2, 3, 5 and 6: The X-ray data for compounds **2** and **6** were collected at 180 K with a Stoe Imaging Plate Diffractometer System (IPDS) equipped with an Oxford Cryosystems cooler device by using a graphite monochromator (λ = 0.71073 Å). Data were collected[14] by using f rotation movement with the crystal-to-detector distance equal to 80 mm (**2**), 70 (**6**) and f = 0.0–250°, Δf = 1.5° (**2**), f = 0.0–200°, Δf = 2.0° (**6**). Crystallographic measurements for **3** and **5** were carried out at 180 K with an Oxford-Diffraction XCALIBUR CCD diffractometer by using graphite-monochromated Mo-K_α radiation. The crystals were placed 50 mm from the CCD detector. More than the hemisphere of reciprocal space was covered by combination of four sets of exposures; each set had a different f-angle (0, 90, 180, 270°). The unit cell determination and data integration were carried out using the CrysAlis package of Oxford Diffraction.[15] All structures were solved by direct methods by using SHELXS-97[16] and refined by full-matrix least-squares on F_o^2 with SHELXL-97[17] with anisotropic displacement parameters for non-hydrogen atoms. All H atoms attached to carbon were introduced in idealized positions (d_{CH} = 0.96 Å) by using the riding model with their isotropic displacement parameters fixed at 120% of their riding atom. Because of statistical disorder of the tetradentate ligand around Fe, the structure of **5** was refined by using a disordered approach in combination with the tools available from the SHELXL97 program package, yielding conformations with respective occupancy factors of 0.74(1) and 0.26(1)*. The molecular plots were obtained using the ZORTEP program.[18] The main crystallographic data together with refinement details are summarized in Table 1. CCDC-639917 for **2**, -639919 for **3**, -639918 for **5** and -639916 for **6**, contain the supplementary crystallographic data for this paper. These data can be obtained free of charge from The Cambridge Crystallographic Data Centre via www.ccdc.cam.ac.uk/data_request/cif.

Supporting Information (see footnote on the first page of this article): Table of the $\chi_M T$ data vs. temperature (T) for complexes **1** and **3**–**6**, Table of the Mössbauer parameters (isomer shift δ, quadrupole splitting ΔE_Q and line width $\Gamma/2$) resulting from fitting the spectra of complexes **1**–**6** and the IR spectra of **1** and the three related complexes.

Acknowledgments

Financial support by the French Ministry for Education, Research, and Technology through a doctoral grant to N. B. and by the CNRS-DFG collaborative programme through a postdoctoral grant to S. S. are gratefully acknowledged.

[1] P. Gütlich, H. A. Goodwin (Eds.), *Topics in Current Chemistry Vol. 233: Spin Crossover in Transition Metal Compounds I*, Springer, Berlin, **2004**, pp. 1–47, and references cited therein.

[2] a) L. J. Wilson, D. Georges, M. A. Hoselton, *Inorg. Chem.* **1975**, *14*, 2968–2975; b) H. Toftlund, S. Yde-Andersen, *Acta Chem. Scand.* **1981**, *A35*, 575–585; c) L. L. Martin, K. S. Hagen, A. Hauser, R. L. Martin, A. M. Sargeson, *J. Chem. Soc. Chem. Commun.* **1988**, *19*, 1313–1315; d) A. H. R. Obaidi, J. J. McGarvey, K. P. Taylor, S. E. J. Bell, K. B. Jensen, H. Toftlund, *J. Chem. Soc. Chem. Commun.* **1993**, *6*, 536–538; e) A. H. R. Al-Obaidi, K. B. Jensen, J. J. McGarvey, H. Toftlund, B. Jensen, S. E. J. Bell, J. G. Carroll, *Inorg. Chem.* **1996**, *35*, 5055–5060; f) Y. Sunatsuki, Y. Ikuta, N. Matsumoto, H. Ohta, M. Kojima, S. Iijima, S. Hayami, Y. Maeda, S. Kaizaki, F. Dahan, J.-P. Tuchagues, *Angew. Chem. Int. Ed.* **2003**, *42*, 1614–1618; g) Y. Ikuta, M. Ooidemizu, Y. Yamahata, M. Yamada, S. Osa, N. Matsumoto, S. Iijima, Y. Sunatsuki, M. Kojima, F. Dahan, J.-P. Tuchagues, *Inorg. Chem.* **2003**, *42*, 7001–7017; h) M. Yamada, M. Ooidemizu, Y. Ikuta, S. Osa, N. Matsumoto, S. Iijima, M. Kojima, F. Dahan, J.-P. Tuchagues, *Inorg. Chem.* **2003**, *42*, 8406–8416; i) Y. Sunatsuki, H. Ohta, M. Kojima, Y. Ikuta, Y. Goto, N. Matsumoto, S. Iijima, H. Akashi, S. Kaizaki, F. Dahan, J.-P. Tuchagues, *Inorg. Chem.* **2004**, *43*, 4154–4171; j) S. Arata, H. Torigoe, T. Iihoshi, N. Matsumoto, F. Dahan, J.-P. Tuchagues, *Inorg. Chem.* **2005**, *44*, 9288–9292; k) N. Bréfuel, S. Imatomi, H. Torigoe, H. Hagiwara, S. Shova, J.-F. Meunier, S. Bonhommeau, J.-P. Tuchagues, N. Matsumoto, *Inorg. Chem.* **2006**, *45*, 8126–8135.

[3] a) O. Kahn, J.-P. Launay, *Chemtronics* **1988**, *3*, 140–151; b) O. Kahn, J. Krober, C. Jay, *Adv. Mater.* **1992**, *4*, 718–728; c) O. Kahn, C. Jay-Martinez, *Science* **1998**, *279*, 44–48.

[4] a) N. Bréfuel, I. Vang, S. Shova, F. Dahan, J.-P. Costes, J.-P. Tuchagues, *Polyhedron* **2007**, *26*, 1745–1757; b) N. Bréfuel, S. Shova, J. Lipkowski, J.-P. Tuchagues, *Chem. Mater.* **2006**, *18*, 5467–5479.

[5] N. N. Greenwood, T. C. Gibbs in *Mössbauer Spectroscopy*, Chapman and Hall, New York, **1971**, pp. 9–11, 50–53.

[6] N. Bréfuel, C. Lepetit, S. Shova, F. Dahan, J.-P. Tuchagues, *Inorg. Chem.* **2005**, *44*, 8916–8928.

[7] P. Gütlich, H. A. Goodwin (Eds.), *Topics in Current Chemistry Vols. 233–235: Spin Crossover in Transition Metal Compounds I–III*, Springer, Berlin, **2004**, and references cited therein.

[8] a) F. Hartmann-Boutron, *Ann. Phys.* **1975**, *9*, 285–356; b) P. Adler, A. Hauser, A. Vef, H. Spiering, P. Gütlich, *Hyperfine Interact.* **1989**, *47*, 343–356; c) P. Adler, H. Spiering, P. Gütlich, *J. Chem. Phys.* **1989**, *50*, 587–597.

[9] a) G. Lemercier, A. Bousseksou, M. Verelst, J.-P. Tuchagues, F. Varret, *J. Magn. Magn. Mater.* **1995**, *150*, 227–230; b) A. Thiel, A. Bousseksou, M. Verelst, F. Varret, J.-P. Tuchagues, *Chem. Phys. Lett.* **1999**, *302*, 549–554.

[10] K. Nakamoto, *Infrared and Raman Spectra of Inorganic and Coordination Compounds*, 4th ed., John Wiley & Sons, New York, **1986**.

[11] N. E. Erikson, N. Sutin, *Inorg. Chem.* **1966**, *5*, 1834–1835.

[12] K. Lagarec, *Recoil, Mössbauer Analysis Software for Windows*, http://www.physics.uottawa.ca/~recoil.

[13] P. Pascal, *Ann. Chim. Phys.* **1910**, *19*, 5–70.

[14] STOE, *IPDS Manual* (Version 2.93), Stoe & Cie, Darmstadt, Germany, **1997**.

[15] *CrysAlis RED* (Version 1.170.32), Oxford Diffraction Ltd., Oxford, U. K., **2003**.

[16] G. M. Sheldrick, *SHELXS-97: Program for Crystal Structure Solution*, University of Göttingen, Göttingen, Germany, **1990**.

[17] G. M. Sheldrick, *SHELXL-97: Program for the Refinement of Crystal Structures from Diffraction Data*, University of Göttingen, Göttingen, Germany, **1997**.

[18] L. Zsolnai, H. Pritzkow, G. Huttner, *ZORTEP – Ortep for PC: Program for Molecular Graphics*, University of Heidelberg, Heidelberg, Germany, **1996**.

Received: March 22, 2007
Published Online: July 30, 2007

